Magnetotransport and magnetocrystalline anisotropy in $Ga_{1-x}Mn_xAs$ epilayers

2007 J. Phys.: Condens. Matter 19 165206

(http://iopscience.iop.org/0953-8984/19/16/165206)

IOP PUBLISHING JOURNAL OF PHYSICS: CONDENSED MATTER

J. Phys.: Condens. Matter **19** (2007) 165206 (11pp) doi:10.1088/0953-8984/19/16/165206

Magnetotransport and magnetocrystalline anisotropy in $Ga_{1-x}Mn_xAs$ epilayers

H X Tang[1] **and M L Roukes**

Condensed Matter Physics 114-36, California Institute of Technology, Pasadena, CA 91125, USA

E-mail: hong.tang@yale.edu and roukes@caltech.edu

Received 22 September 2006, in final form 11 December 2006
Published 6 April 2007
Online at stacks.iop.org/JPhysCM/19/165206

Abstract

We present an analysis of the magnetic anisotropy in epitaxial $Ga_{1-x}Mn_xAs$ thin films through electrical transport measurements on multiterminal microdevices. The film magnetization is manipulated in 3D space by a three-axis vector magnet. Anomalous switching patterns are observed in both longitudinal and transverse resistance data. In transverse geometry in particular we observe strong interplay between the anomalous Hall effect and the giant planar Hall effect. This allows direct electrical characterization of magnetic transitions in the 3D space. These transitions reflect a competition between cubic magnetic anisotropy and an effective out-of-plane uniaxial anisotropy, with a reversal mechanism that is distinct from the in-plane magnetization. The uniaxial anisotropy field is directly calculated with high precision and compared with theoretical predictions.

(Some figures in this article are in colour only in the electronic version)

Ferromagnetic semiconductors have demonstrated a variety of interesting properties arising from strong coupling between local spins and hole carriers [1]. There has been intense interest in the magnetic anisotropy in the $Ga_{1-x}Mn_xAs$ magnetic semiconductors [2–8]. A theory based on the mean-field Zener model predicts magnetic anisotropy induced by the lattice strain present in epitaxial ferromagnetic semiconductor layers [9, 10], with compressive and tensile strain inducing in-plane and out-of-plane magnetization. However, experiments to date can only provide crude estimates of the strength of the strain induced magnetic anisotropy fields and do not have sufficient resolution to validate the theoretical predictions. Furthermore, fundamental understanding of magnetic domain structures requires a more accurate knowledge of magnetic anisotropies. In this paper, we report on magnetic anisotropy studies based upon anomalous perpendicular Hall and magnetoresistance transitions in microfabricated

[1] Present address: Departments of Electrical and Mechanical Engineering, Yale University, New Haven, CT 06520, USA.

$Ga_{1-x}Mn_xAs$ multiterminal microdevices. The manifested magnetic transitions are interpreted based on competition between strain induced out-of-plane uniaxial anisotropy and crystalline cubic anisotropy. All relevant magnetic anisotropy fields are obtained with high precision.

$Ga_{1-x}Mn_xAs$ epilayers grown on GaAs substrate are under compressive lattice-mismatching strain, and as a result they have strong in-plane magnetic anisotropy [1]. In a previous paper [11] we reported the enormous spontaneous Hall resistance jumps in $Ga_{1-x}Mn_xAs$ microjunctions subjected to a sweeping in-plane magnetic field. This giant planar Hall effect (GPHE) was qualitatively explained by macroscopic-scale domain reversal governed by the combined effect of a dominant cubic anisotropy and a weak uniaxial in-plane anisotropy field of unknown origin. Both the cubic anisotropy field and this weak in-plane anisotropy field were derived from magnetotransport measurement data.

The intriguing giant planar Hall effect in $Ga_{1-x}Mn_xAs$ encouraged us to explore the magneto-electric effect with magnetization oriented other than in-plane, such as a conventional Hall measurement where the field is applied perpendicular to the films. Sample preparation and our experimental setup were described in an earlier publication [11].

For a single-domain magnetic conductive material with the application of magnetic field **H** and current density **j**, the electrical field in the sample is given by [12, 13]

$$\mathbf{E} = \rho_\perp \mathbf{j} + (\rho_\parallel - \rho_\perp)(\mathbf{j}\cdot\hat{\mathbf{m}})\hat{\mathbf{m}} + (R_0\mathbf{H} + R_S 4\pi\mathbf{M}) \times \mathbf{j}, \tag{1}$$

where $\hat{\mathbf{m}}$ is a unit vector directed along the magnetization **M**, R_0 is the normal Hall resistivity and R_S is an anomalous Hall effect coefficient. In this equation, the first two terms contribute to the longitudinal magnetoresistance and the planar Hall effect observed in this material [11]. The third and the fourth term represent the normal Hall effect and anomalous Hall effect (AHE), respectively. For ferromagnets with free carriers, the anomalous coefficient R_S is in many cases much greater than the ordinary coefficient R_0, which is $1/pe$ in a hole doped magnetic semiconductor. For example, in the $Ga_{1-x}Mn_xAs$ epilayers studied in this work, the hole density is pretty high ($\sim 10^{20}$ cm^{-3}) and the ordinary Hall resistance is estimated to be 0.2 mΩ Oe^{-1}. This makes the direct influence of the external field on Hall resistance negligible in the experimental low field region; thus, for the sake of simplicity in the remainder of the paper we shall only consider the contribution of the anomalous Hall effect when sample is subject to a perpendicular field. From equation (1) the transverse and longitudinal components of the vector **E** are

$$E_x = j\rho_\perp + j(\rho_\parallel - \rho_\perp)\sin^2\theta\cos^2\varphi, \tag{2}$$

$$E_y = j(\rho_\parallel - \rho_\perp)\sin^2\theta\sin\varphi\cos\varphi + j(R_0 H_\perp + R_S 4\pi M_S\cos\theta). \tag{3}$$

These expressions are made using the coordinate system shown in figure 1 where the external electric field is applied along the x direction and the polar angle θ and azimuthal angle φ specify the orientation of the magnetic moment. If the planar Hall effect is the only term to be investigated then the magnetic field is applied in the plane of the film to ensure that $M_\perp$ is zero. The intention in this section, however, is to measure the magnetoresistance when the field is applied at some angle to the film plane. In this case $M_\perp$ is not zero and the anomalous Hall effect has to be taken into account.

1. Out-of-plane transport measurement results

Figure 2 shows the longitudinal magnetoresistance R_{sheet} measured at 4.2 K for a magnetic field oriented along the z direction and along two orthogonal in-plane angles (20° off x and y, respectively). The field sweep range is ± 1 T. At higher fields there is a large overall negative magnetoresistive for all three field orientations, consistent with the suppression of localization

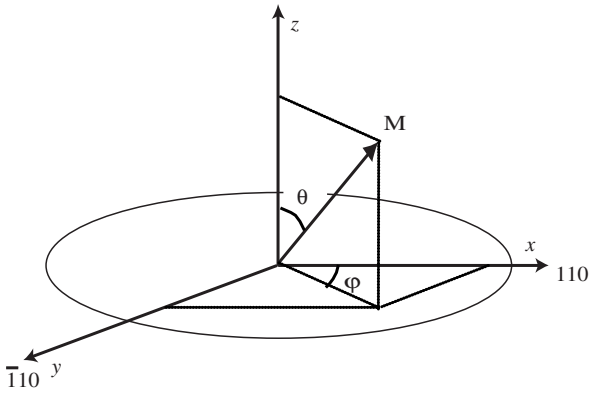

Figure 1. Coordinate system in 3D space for out-of-plane experiments.

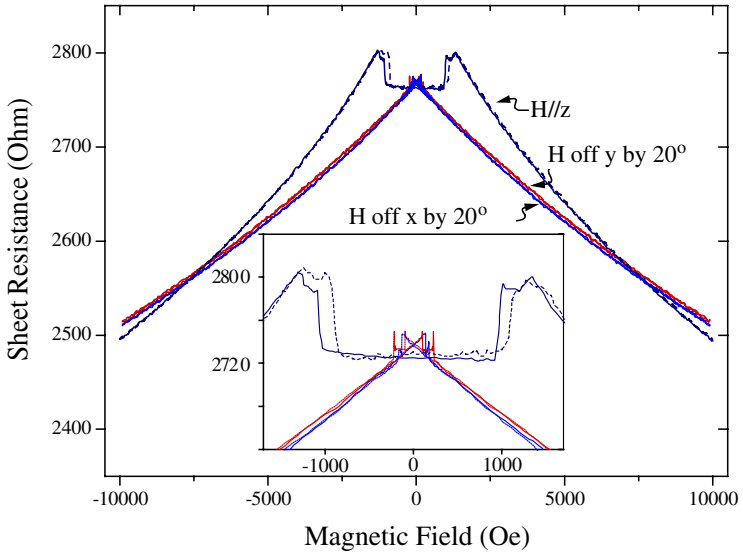

Figure 2. Longitudinal resistance R_{sheet} for external fields applied in three orthogonal orientations: out-of-plane ($H \parallel z$), in-plane 20° off x axis, in plane 20° off y axis. The result for a planar Hall resistance R_{PHE} is also presented. Inset: enlarged view of low field magnetoresistance in the low field region.

in the studied sample [14]. The normal sheet resistance exhibits a pan-shape in the low field region, with jumps at about ±1300 Oe and a flat magnetoresistance region between them. These jumps are associated with the reorientation of the sample magnetization between the perpendicular direction and the in-plane direction. An enlarged view of sheet resistance in the field range ±1500 Oe is reproduced in the inset of figure 2. The resistance change is ∼35 Ω, about half the size of the planar Hall resistance jumps (72 Ω) at this temperature.

Figure 3 shows the Hall resistance R_{H} measured as a function of perpendicular field. For comparison, the planar Hall resistance loop at 20° off the [110] axis is also presented. At large negative field, the anomalous Hall resistance saturates, corresponding to a saturated magnetization along the $-z$ direction. This justifies our assumption that the ordinary Hall contribution is *negligible* in this field range. On sweeping the field up, a broad AHE resistance

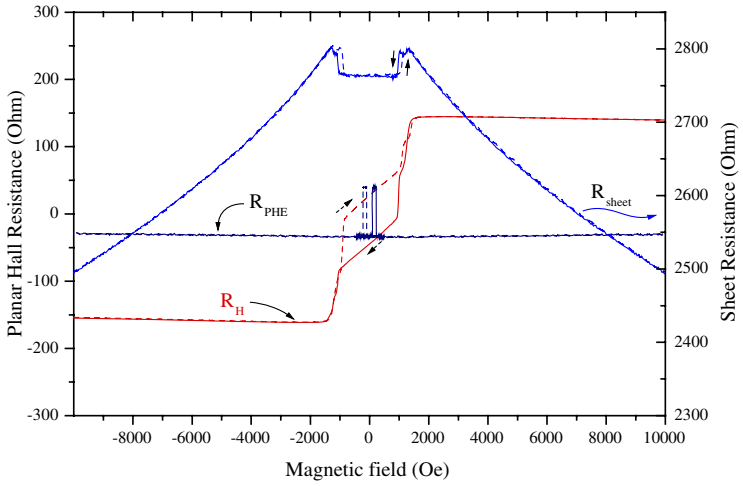

Figure 3. Longitudinal resistance R_{sheet} and Hall resistance R_{H} for a 100 μm wide Hall bar subject to a perpendicular field. For comparison, the result for a planar Hall resistance R_{PHE} is also presented.

jump starts at around -1500 Oe and ends at -1000 Oe. Then the normal Hall resistance varies linearly before a second jump arises at 1000 Oe. The magnetization is fully reversed at 1500 Oe and saturates again beyond this field intensity. It is apparent that the transition processes in both transverse measurement and longitudinal measurement are simultaneous and related. The total AHE resistance change is 306 Ω, i.e.

$$4\pi M R_{\text{S}} = 153\ \Omega. \tag{4}$$

From which, using $4\pi M = 493$ Oe measured by a SQUID magnetometer, an anomalous resistance coefficient $R_{\text{S}} = 0.3\ \Omega\ \text{Oe}^{-1}$ can be deduced. When ramping down the field, a large hysteresis occurs in the field range of ± 1000 Oe. It is worth mentioning that this hysteresis around zero field does not appear in each sample we studied. If present, the difference in normal Hall resistance between the two hysteresis curves matches the magnitude of the planar Hall resistance jumps. This matching is repeatable in all the samples we have measured. Hence we believe that this hysteresis originates from different in-plane magnetization orientations when the magnetic field is swept across zero magnetic field.

2. Modelling of the perpendicular magnetization reversal process

In planar geometry, a model based upon a mixture of cubic anisotropy and a weak in-plane anisotropy can be used to explain the unusual switching behaviour in the planar Hall resistance measurements [11]. Anisotropy constants—the ratio between anisotropy energy and magnetization—are deduced from transport measurement data. As one can imagine, in a perpendicular magnetic field, in addition to the conventional in-plane and out-of-plane uniaxial anisotropy fields, the magnetic moment should also be under the influence of the two out-of-plane cubic easy axes. Unfortunately, unlike the purely uniaxial anisotropy, the case of cubic magnetocrystalline anisotropy was not fully explored before, even though it represents a lot of important materials. A full description of the magnetization reversal process needs to contain precisely all types of magnetic energy contribution. The following expression describes

a complete free energy for magnetization in 3D space:

$$E = K_{\mathrm{ui}}\left(\frac{\mathbf{M}\cdot\mathbf{u}_i}{M_{\mathrm{s}}}\right)^2 + K_{\mathrm{uo}}\left(\frac{\mathbf{M}\cdot\mathbf{n}}{M_{\mathrm{s}}}\right)^2 + K_1(\alpha_1^2\alpha_2^2 + \alpha_2^2\alpha_3^2 + \alpha_3^2\alpha_1^2) + 2\pi(\mathbf{M}\cdot\mathbf{n})^2 - \mathbf{M}\cdot\mathbf{H} \tag{5}$$

where the direction cosines $(\alpha_1, \alpha_2, \alpha_3) = (M_x/M, M_y/M, M_z/M)\cdot\mathbf{n}$ is the out-of-plane unit vector, and $\mathbf{u}_i$ is a unit vector defining the in-plane anisotropy orientation. K_{ui} and K_{uo} are in-plane and out-of-plane uniaxial anisotropy constants, respectively. For $Ga_{1-x}Mn_xAs$ thin film grown on a low temperature GaAs substrate, K_{ui} has a negative value and K_{uo} is positive. K_1 is the cubic anisotropy constant, and the higher order magnetocrystalline energy contributions are ignored. The fourth term is the magnetostatic energy, i.e. demagnetization field induced shape anisotropy. The last term represents the Zeeman energy. As we have shown in [11], the in-plane uniaxial anisotropy is very weak; hence in the analysis of out-of-plane magnetization reversal, for simplicity we will abandon this term. The out-of-plane uniaxial anisotropy, originating from the compressive strain that exists at the $Ga_{1-x}Mn_xAs$/GaAs interface, favours the alignment of magnetization in the plane and accordingly has a positive value. One theoretical calculation predicted a value of the uniaxial anisotropy field of about 3000 Oe [9]. Combining it with the shape anisotropy, an effective out-of-plane uniaxial anisotropy energy can be defined as

$$E_{\mathrm{u}} = 2\pi\left(1 + \frac{2K_{\mathrm{uo}}}{4\pi M_{\mathrm{s}}^2}\right)(\mathbf{M}\cdot\mathbf{n})^2 = 2\pi\eta(\mathbf{M}\cdot\mathbf{n})^2 \tag{6}$$

where $\eta = 1 + \frac{H_{\mathrm{uo}}}{4\pi M_{\mathrm{s}}}$ would be a number of the order of 10 (in our sample $4\pi M_{\mathrm{s}} = 500$ Oe). Here H_{uo} is the out-of-plane uniaxial field, defined by $H_{\mathrm{uo}} = \frac{2K_{\mathrm{uo}}}{M_{\mathrm{s}}}$. By using the coordinate system depicted in figure 1, for a field $\mathbf{H}$ applied perpendicular to the film, the magnetic free energy density is written as

$$E(\theta, \varphi) = \tfrac{1}{4}K_1(\sin^4\theta\cos^2 2\varphi + \sin^2 2\theta) + 2\pi\eta M^2\cos^2\theta - MH\cos\theta. \tag{7}$$

Since the field is applied along the z direction, no additional variable is needed to describe its orientation. The stable equilibrium conditions can be expressed in polar coordinates as

$$\frac{\partial E}{\partial\theta} = 0, \tag{8}$$

$$\frac{\partial E}{\partial\varphi} = 0, \tag{9}$$

$$\frac{\partial^2 E}{\partial\theta^2}\frac{\partial^2 E}{\partial\varphi^2} - \left(\frac{\partial^2 E}{\partial\varphi^2}\right)^2 > 0, \tag{10}$$

$$\frac{\partial^2 E}{\partial\varphi^2} > 0. \tag{11}$$

These equations put a restriction on the angle φ of the equilibrium position

$$\cos 2\varphi = 0, \tag{12}$$

which is the same as the in-plane situation. Depending on the magnetization history, the magnetization remains in the directions of minimum energy with $\varphi = 45°$, 135°, 215° or 305°. The weak in-plane uniaxial anisotropy may cause the actual φ orientations to deviate by a very small angle from those angles. An effective one-dimensional energy density can be found by substituting the value determined by equation (12) into equation (7):

$$E_{\mathrm{eff}}(\theta) = \tfrac{1}{4}K_1\sin^2 2\theta + 2\pi\eta M^2\cos^2\theta - MH\cos\theta. \tag{13}$$

This free energy density expression is analogous to the in-plane energy density (equation (1) in [11]), but with opposite signs for both the cubic term and the uniaxial term. Here

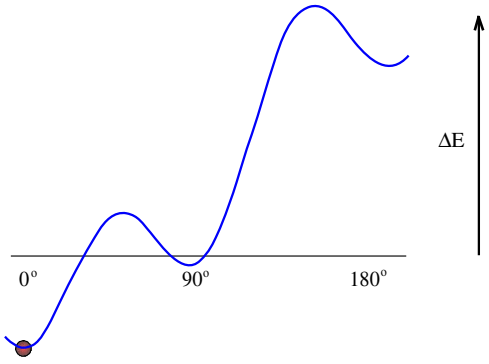

Figure 4. An illustration of three energy minima for out-of-plane free energy. The horizontal axis is the polar angle. In this particular diagram a large positive field is applied.

the out-of-plane uniaxial anisotropy is much stronger than the in-plane uniaxial anisotropy. The competition between this uniaxial anisotropy and cubic anisotropy provides a unique magnetization reversal process and is able to account for all the anomalous normal magnetoresistance behaviour. At zero external field, the stable solutions for θ are multiples of 90°. Since θ is in the range of [0°, 180°], instead of four equilibrium orientations, now only three exist at zero field: 0°, 90° and 180°. For nonzero external field, they may move away from these angular values and can be solved directly from equations (8)–(11) or from the analysis of the effective energy density described by equation (13):

$$M \sin\theta\{H - [(H_{cA} + 4\pi\eta M)\cos\theta - 2H_{cA}\cos^3\theta]\} = 0 \tag{14}$$

$$H_{cA}\cos 4\theta - 4\pi\eta M \cos 2\theta + H\cos\theta > 0. \tag{15}$$

Here $H_{cA} = 2|K_1|/M$ is the cubic anisotropy field whose value has been obtained through planar Hall resistance measurements. Equation (14) gives

$$\sin\theta = 0 \Rightarrow \theta_1 = 0^\circ, \qquad \theta_3 = 180^\circ \tag{16}$$

$$\theta_2 = 90^\circ - \delta_0, \qquad \text{with } (H_{cA} + 4\pi\eta M)\sin\delta_0 = H + 2H_{cA}\sin^3\delta_0. \tag{17}$$

The first two solutions are north/south poles in polar coordinates, representing a saturated out-of-plane magnetization. The third solution is a close to plane solution ($\theta \sim 90^\circ$). The direction to which the magnetization is directed is determined by the criteria equation (15) and the magnetic history. Figure 4 exemplifies the situation when a large positive magnetic field is applied. In such a case, magnetization is saturated in the positive z direction and θ coordinate stays at zero (θ_1).

We use the analysis of the magnetic anisotropy energy in equation (13) as a basis for understanding the abnormal magnetization reversal shown in figure 3. In a high positive field, the magnetization saturates at $\theta = \theta_1$, which is the only stable solution. On reducing the magnetic field, a new stable magnetization orientation $\theta = \theta_2$ starts to develop. In the presence of thermal excitation and interaction of local defects, magnetic domains can be launched in this new polarization. This nucleation field is hereafter referred to as H_N and is defined by

$$\frac{\partial^2 E(\theta, H_N)}{\partial\theta^2} = 0 \qquad \text{and} \qquad \frac{\partial E(\theta, H_N)}{\partial\theta} = 0. \tag{18}$$

Simple calculus yields

$$H_{C1} = H_N = \frac{\sqrt{6}H_{cA}}{9}\left(1 + \frac{4\pi\eta M}{H_{cA}}\right)^{3/2}. \tag{19}$$

This critical field has its direct origin from the cubic anisotropy energy surface of $Ga_{1-x}Mn_xAs$. There is no correspondence in a conventional magnetic material with uniaxial anisotropy, evident from the fact that H_{C1} approaches infinity when H_{cA} goes to zero.

The domains of the second phase grow continuously on further reducing the field. Note that for perpendicularly magnetized films, the energetics is different from the in-plane situation, where single domain behaviour appears on a macroscopic scale and magnetization switching is achieved through domain wall nucleation, depinning and subsequent sweeping through the sample. A distinct domain wall pinning energy density has to be overcome in the switching process. For perpendicular magnetization the final magnetization states are continuously distributed and the domain wall pinning energy cannot be described by a definite value. The difference in magnetic domain structure for perpendicular magnetized films and in-plane magnetized films has been observed by scanning Hall microscopy and scanning SQUID microscopy at low temperature [15]. The film with perpendicular magnetization has a maze domain structure more similar to those of conventional ferromagnetic materials, whereas the film with in-plane magnetization has unconventional domain structures that show no evidence of a domain wall in a fairly large area (about 300 μm by 300 μm). Therefore upon decreasing the external field, once the free energy at θ_2 matches that of θ_1, i.e. $E = 0$ in equation (13), domain wall nucleation processes terminate and all domains fall into this new, more favourable stable configuration and eliminate domain structure on a fairly large scale. Coherent domain wall rotation starts to dominate magnetization reorientation. This critical field H_{C2}, can be obtained by solving the equation

$$E(\theta = 0, H = H_{C2}) = E(\theta = \theta_2, H = H_{C2}). \tag{20}$$

For $H_{cA} = 0$, i.e. only uniaxial anisotropy terms are present, this equation gives $H_{C2} = 4\pi\eta M$, in agreement with the coercivity predicted by the Stoner–Wohlfarth model for uniaxial crystalline anisotropic materials. For nonzero H_{cA} values, the root is not straightforward. An analytical solution does exist but it is very complicated. For large H_{cA}, by expanding $\cos(\theta)$ to the second order of θ, a nice approximation can be derived:

$$H_{C2} = 2\pi\eta M\left[1 + \frac{1}{2(1 + H_{cA}/4\pi\eta M)}\right]. \tag{21}$$

This is the initial field of the linear normal Hall resistance in figure 3. Hereafter the magnetization starts to evolve coherently with external field according to equation (17). In this region, it is more convenient to express **M** in terms of its out-of-plane component

$$H = (H_{cA}/M + 4\pi\eta)M_\perp + 2H_{cA}M_\perp^3/M^3. \tag{22}$$

Since $M_\perp \sim 0$, the third-order term can be ignored. Consequently the perpendicular component of magnetization is a linear function of external field

$$M_\perp = H/(H_{cA}/M + 4\pi\eta). \tag{23}$$

Again, in the limit of $H_{cA} = 0$, the conventional uniaxial magnetic behaviour is restored. For magnetic moments close to in-plane orientations, the cubic anisotropy field effectively combines with uniaxial anisotropy fields and behaves like an ordinary uniaxial magnet with regards to the z-component of the magnetization. This linear dependence of the perpendicular component of **M** around zero external field has been observed by SQUID measurements. The spin polarization of $Ga_{1-x}Mn_xAs$ determined by the spin-LED method has also demonstrated a similar behaviour [16].

This linear evolution of magnetization comes to an end at an external field $H_{C3} = -H_{C2}$ where its energy matches the magnetic energy at $\theta = \theta_3$. Following that, a nucleation process to create domains θ_3 dominates. This nucleation process persists until the intermediate state

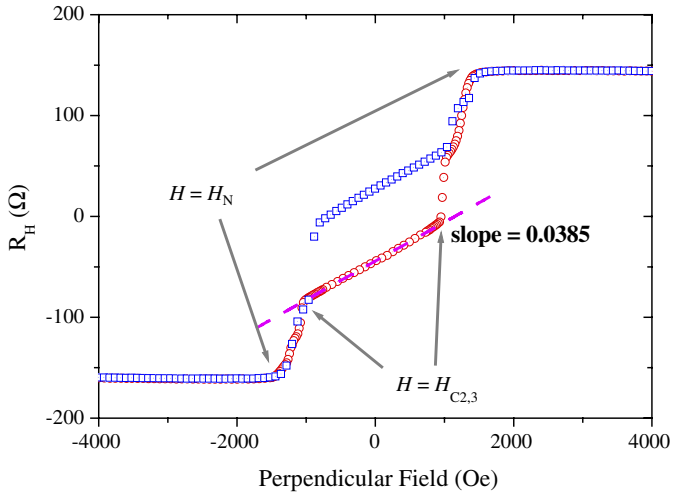

Figure 5. Characteristic fields for films with perpendicular field: nucleation fields, $\pm H_{\rm N}$, and domain annihilation fields, $H_{\rm C2,3}$. Magnetization precesses coherently in the linear Hall resistance region close to zero field.

$\theta = \theta_2$ vanishes at a large negative threshold field $H_{\rm C4} = -H_{\rm C1}$. Domain walls disappear beyond this field and the magnetization reversal is accomplished.

Both longitudinal magnetoresistance and normal Hall resistance shown in figures 2 and 3 can be explained by the preceding analysis of the magnetization process. In a down-swept field, the overall transition sequence of θ coordinate is summarized as $\theta = 0^\circ \rightarrow$ nucleation, $\rightarrow \theta = \theta_2 \sim 90^\circ$, coherent rotation, $\rightarrow$ nucleation $\rightarrow \theta = 180^\circ$. For longitudinal resistance, $\sin^2\theta$ in equation (2) changes from 0 to a value close to 1 then back to 0. From equation (2), the size of the two jumps is $|\rho_\parallel - \rho_\perp|/2 \sim 36\ \Omega$, consistent with the observed value. In the $\theta \sim \theta_2$ region, θ deviates from 90° by a small number, therefore according to equation (2) the sheet resistance exhibits an almost constant value that matches the sheet resistance with in-plane magnetization (figure 2 inset). The two jumps in the normal Hall resistance and normal sheet resistance reflect the magnetization transitions from 0° to ∼90° and from ∼90° to 180°. The nucleation starts at around 1460 Oe ($H_{\rm N}$) and ends at about 990 Oe ($H_{\rm C2}$). Employing simulated $H_{\rm cA} = 2400$ Oe in [11], we estimate $4\pi\eta M = 1635 \pm 65$ Oe.

A more accurate value can be deduced by fitting to the linear part of the Hall resistance. To first order in $M_\perp$, the Hall resistance in equation (3) gives

$$R_{\rm H} = R_{\rm S} 4\pi M_\perp. \tag{24}$$

By applying equation (4) and equation (24) we have

$$R_{\rm H} = \frac{R_{\rm S} 4\pi M}{H_{\rm cA} + 4\pi\eta M} H = \frac{303\ \Omega/2}{H_{\rm cA} + 4\pi\eta M} H. \tag{25}$$

A typical fitting is presented in figure 5, indicating $H_{\rm ca} + 4\pi\eta M = 3972$ Oe. And the effective uniaxial anisotropy field is

$$4\pi\eta M = 1572\ \text{Oe}. \tag{26}$$

The value of η is found to be 3.1, giving a perpendicular uniaxial anisotropy field of 1072 Oe.

Our next task is to understand the hysteresis behaviour in the low field region of the normal Hall resistance data. The fact that the resistance difference matches the value of the planar

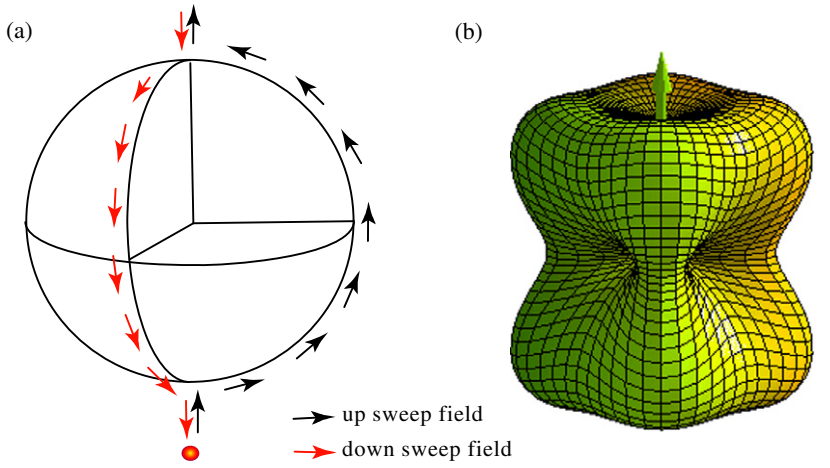

Figure 6. Illustration of the origin of hysteresis in out-of-plane Hall measurement. (a) When the perpendicular magnetic field sweeps up and down across the zero, the in-plane magnetizations are orthogonal, giving a resistance difference the same as the spontaneous planar Hall resistance jumps. (b) Plot of magnetic anisotropy surface in 3D space.

Hall resistance jumps convinces us that the magnetization must follow a trajectory depicted in figure 6(a). As illustrated, the magnetization curve falls into different stable trajectories with orthogonal φ values. When the perpendicular field is swept across zero, the in-plane angles are normal to each other for the up-sweep cycle and the down-sweep cycle, producing a resistance difference the same as that for the spontaneous planar Hall resistance jumps. We attribute the hysteresis to uncontrolled misalignment of the vertical magnetic field with the film normal or the remnant fields of in-plane split magnet pairs. If the external field is applied exactly along the film normal, the magnetization trajectory will be random. But in all our experiments, once set up, reproducible hysteresis patterns are observed on all samples. Suppose the external field is slightly tilted away from the firm normal by coordinates (θ_0, φ_0), then equation (5) is rewritten as

$$E(\theta,\varphi) = \tfrac{1}{4}K_1 \sin^4\theta\cos^2 2\varphi - MH\sin\theta\sin\theta_0\cos(\varphi-\varphi_0) + \tfrac{1}{4}K_1\sin^2 2\theta + 2\pi\eta M^2\cos^2\theta - MH\cos\theta\cos\theta_0. \quad (27)$$

The terms containing angle φ is similar to the in-plane magnetic anisotropy energy with cubic energy replaced by $K_1\sin^4\theta$ and the effective magnetic field replaced by $H\sin\theta\sin\theta_0$. The φ coordinate evolution depends on the ratio between these coefficients, whose values vary significantly on approaching the poles. It is not surprising that, for an external field not perfectly aligned along the field normal, the magnetization φ coordinate will switch alternatively along possible configurations in successive field cycles.

3. Magnetic sweep in an arbitrary direction in 3D space: a mixture of the anomalous Hall effect and the planar Hall effect

The model we present above can be verified by sweeping a magnetic field in 3D space. By programming the vector magnet, we tilt the magnetic field off from the orientation direction with azimuthal angle φ fixed at 15° off the [110] direction. In figure 7, the measured Hall resistance is shown as a function of the magnetic field component along the x axis.

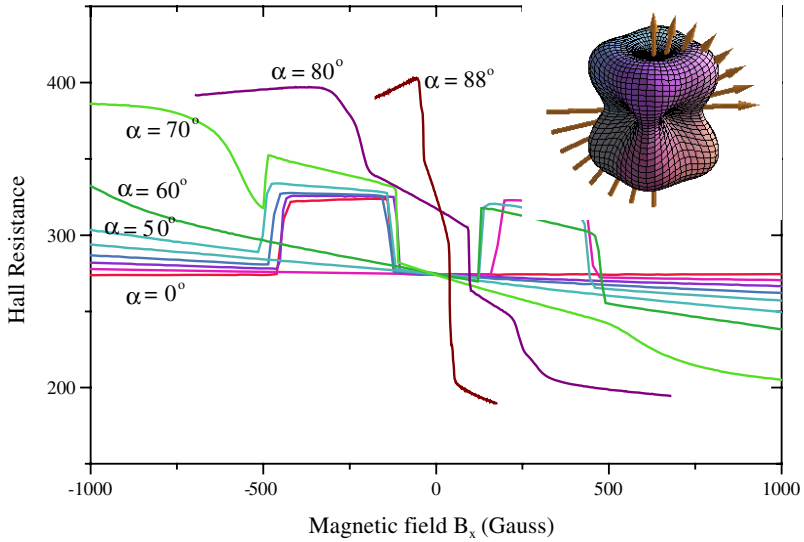

Figure 7. When magnetic field is swept across zero along an arbitrary direction in 3D space, the Hall resistance shows evolution from out-of-plane behaviour to an in-plane planar Hall effect behaviour.

At angles larger than 80°, the Hall resistance shows similar behaviour to that of out-of-plane measurement. When the magnetic field tilt angle becomes smaller than 80°, in-plane energy minima become accessible in the field span. Therefore, complex transition patterns involving both out-of-plane and in-plane easy axes start to develop. As expected, in figure 7, at intermediate tilt angle, a mixture of anomalous Hall resistance and planar Hall resistance appears. When the magnetic field lies completely in the plane, the out-of-plane easy axis becomes inaccessible and only planar Hall transitions remains.

In conclusion, through planar Hall resistance and normal Hall resistance measured at liquid helium temperature, we have deduced all the magnetic anisotropy fields: the cubic anisotropy field, 2400 Oe, the in-plane uniaxial anisotropy field, 133 Oe (along [110]), the out-of-plane uniaxial anisotropy field, 1072 Oe. To our knowledge, this kind of technique has not been established before. The deduced out-of-plane uniaxial anisotropy field is significantly less than the theoretical prediction made by Dietl *et al* [9]. Systematic study of magnetic anisotropy on $Ga_{1-x}Mn_xAs$ epilayers with varying thickness and Mn concentration will enable further examination of existing theories regarding the origin of the mechanism of magnetic anisotropy and ferromagnetism. Meanwhile, we have measured the spontaneous magnetoresistance anisotropy constant $\rho_\perp - \rho_\parallel \sim -72\ \Omega$, and the anomalous Hall resistance coefficient $4\pi M R_S = 153\ \Omega$. Both of them have their origins in the spin–orbit interaction; it is not clear how these numbers are related.

Acknowledgments

We acknowledge support from DARPA under grants DSO/SPINS-MDA 972-01-1-0024.

References

[1] Ohno H 1998 *Science* **281** 951 and references therein
[2] Moore G P, Ferré J, Mougin A, Moreno M and Däweritz L 2003 *J. Appl. Phys.* **94** 4530

[3] Hamaya K, Moriya R, Oiwa A, Taniyama T, Kitamoto Y, Yamazaki Y and Munekata H 2004 *Japan. J. Appl. Phys.* **43** L306
[4] Takamura K, Matsukura F, Chiba D and Ohno H 2002 *Appl. Phys. Lett.* **81** 2590
[5] Matsukura F, Sawichi M, Dietl T, Chiba D and Ohno H 2004 *Physica* E **21** 1032
[6] Kreutz T C, Allen W D, Gwinn E G, Awschalom D D and Gossard A C 2004 *Phys. Rev.* B **69** 081302
[7] Welp U, Vlasko-Vlasov V K, Liu X, Furdyna J K and Wojtowicz T 2003 *Phys. Rev. Lett.* **90** 167206
[8] Liu X, Sasaki Y and Furdyna J K 2003 *Phys. Rev.* B **67** 205204
[9] Dietl T, Ohno H and Matsukura F 2001 *Phys. Rev.* B **63** 195205
[10] Abolfath M, Jungwirth T, Brum J and MacDonald A H 2001 *Phys. Rev.* B **63** 054418
[11] Tang H X, Kawakami R K, Awschalom D D and Roukes M L 2003 *Phys. Rev. Lett.* **90** 107201
[12] Ogrin F Y, Lee S L and Ogrin Y F 2000 *J. Magn. Magn. Mater.* **219** 331
[13] McGuire T and Potter R I 1975 *IEEE Trans. Magn.* **11** 1018
[14] Iye Y, Oiwa A, Endo A, Katsumoto S, Matsukura F, Shen A, Ohno H and Munekata H 1999 *Mater. Sci. Eng.* B **63** 88
[15] Fukumura T *et al* 2001 *Physica* E **10** 135
[16] Young D K, Johnston-Halperin E, Awschalom D D, Ohno Y and Ohno H 2002 *Appl. Phys. Lett.* **80** 1598